

# Slip-velocity and drag of large neutrally-buoyant particles in turbulent flows

**G Bellani and E A Variano**

Department of Civil and Environmental Engineering, University of California,  
Berkeley, CA 94720, USA

E-mail: [bellani@berkeley.edu](mailto:bellani@berkeley.edu)

**Abstract.** We discuss possible definitions for a slip velocity that describes the relative motion between large particles and a turbulent flow. This definition is necessary because the slip velocity used in the standard drag model fails when particle size falls within the inertial subrange of ambient turbulence. By decomposing drag into steady and stochastic components, we obtain both a steady slip velocity and a fluctuating slip velocity. From this decomposition, we propose two definitions for stochastic slip velocity. These definitions were selected in part due to their simplicity: they do not require filtration of the fluid phase velocity field, nor do they require the construction of conditional averages on particle locations. A key benefit of this simplicity is that the stochastic slip velocity proposed here can be calculated equally well for laboratory, field, and numerical experiments. The stochastic slip velocity allows the definition of a Reynolds number that should indicate whether large particles in turbulent flow behave (a) as passive tracers; (b) as a linear filter of the velocity field; or (c) as a nonlinear filter to the velocity field. We calculate the value of stochastic slip for ellipsoidal and spherical particles (the size of the Taylor microscale) measured in laboratory homogeneous isotropic turbulence. The resulting Reynolds number is significantly higher than 1 for both particle shapes, and velocity statistics show that particle motion is a complex non-linear function of the fluid velocity. We further investigate the nonlinear relationship by comparing the probability distribution of fluctuating velocities for particle and fluid phases.

## 1. Introduction

It is well known that particles suspended in a turbulent flow can significantly modulate the turbulent dynamics even at moderate concentrations [1, 2, 3]. The ability to predict turbulence modulation by particles (change in Turbulent Kinetic Energy (TKE), dissipation, etc.), as well as the dynamics of the suspended particles (aggregation-dispersion mechanisms, encounter rates, etc.) strongly depends on our ability to predict the forces that the individual particles experience in turbulent flows.

However, quantifying the forces mediating fluid-particle coupling is nontrivial. Neither the stochastic nor deterministic description of turbulent suspensions is currently at the level required for useful engineering predictions. The limits of current knowledge were summarized eloquently by Qureshi *et al.* [4]: “[...] writing (not to mention solving) the particle equation of motion in the most general case remains a challenge, and only limited cases are treated at present.”

The forces which explicitly couple fluid and particle phases are the shear and normal stresses felt at the particle–fluid boundary. Many prediction schemes attempt to simplify the description by replacing the integral of surface forces with a local body force, the familiar drag force  $F_D$ . This method works well when particles move through a steady flow with a predictable wake structure. However, drag models lose their predictive ability when the particle wake is strongly influenced by stochasticity in the fluid phase (most notably fluid turbulence). New models are needed, as discussed below. When formulating these new models, it is common to use ideas and formulas carried over from the simpler flows in which the standard drag model works well. One such idea is slip velocity, which is clearly defined in the simple drag model, but becomes problematic in turbulent flows. Our goal in this paper is to specify a stochastic slip velocity in a general and unambiguous manner. Doing so will advance the community’s ability to formulate drag models predicting particle–fluid coupling.

## 2. Background

The Stokes drag for a sphere in a creeping flow is:

$$F_D = 3\pi\mu_f d_p U_s = \alpha U_s, \quad (1)$$

where  $d_p$  is particle diameter and  $U_s$  is the slip velocity  $U_s = U_f - U_p$ , where  $U_f$  is an appropriate fluid velocity and  $U_p$  is an appropriate particle velocity. For equation (1),  $U_s$  is defined as the difference between particle center-of-mass velocity  $u_p$  and the uniform velocity found outside the particle  $u_\infty$ . When the particle Reynolds number  $Re_p \equiv U_s d_p \nu^{-1} > \approx 1$ , equation (1) becomes inaccurate because of nonlinearities that appear in the drag due to boundary layer separation. These are quantified with empirical correction factors, such as  $\beta = (1 + 0.15 Re_p^{0.687})$  [5] which appears in the drag model as:

$$F = \alpha U_s \beta(U_s), \quad (2)$$

Neither equation (1) nor equation (2) is valid for nonuniform flows. In the case of simple shear, some extensions are possible. Turbulence, however, is far more complicated, for the flow exerts time-varying stresses on the particle surface that are completely different from those due to boundary layer separation in uniform flow. The resultant force on a particle then includes a history term and an inertial term that depend on particle–fluid relative accelerations [6, 7].

Small particles often experience small relative acceleration, and see the turbulent stresses as uniform and linear fields. As a result equations (1) and (2) stay approximately true. The slip velocity in this case can be defined as the instantaneous difference between the particle’s Lagrangian velocity  $u_{pL}$  and the co-located Eulerian velocity of the fluid  $u_f$ , giving  $U_{SE-L} \equiv u_f - u_{pL}$ . This definition works because the fluid velocity field can be considered ‘unbroken’ by the presence of the particles.  $U_{SE-L}$  is used in numerical models that perform Lagrangian tracking of infinitesimally small particles through Eulerian velocity fields [3]. The results have led to some significant advances in understanding, but also deserve a significant amount of caution, as discussed in [8].

Larger particles experience nonuniform stress fields due to turbulence. There may be some large lengthscale at which the turbulent field can be filtered such that the particle responds to the filtered velocity field  $\hat{u}_f$  according to the drag law:

$$F_d = \alpha \hat{U}_s \beta (\hat{U}_s). \quad (3)$$

However, the particle will also experience drag due to the sub-filter-scale stresses. This additional drag will be relevant to processes such as particle collisions and fluid TKE modulation. The form of the sub-filter-scale terms is far from trivial, as expressions for history and inertial terms due to the unsteadiness are complex and their analytical expression has only been derived for the special cases of tiny particles moving with small slip velocities [9]. The work of Bagchi & Balachandar [10] provides a good foundation for understanding the effect of particle size and turbulence intensity. In this work, the authors explored the case in which a particle is unmoved by any turbulent fluctuations, but rather stays fixed as a turbulent flow advects past at a constant speed. They use direct numerical simulation (DNS) to exactly determine drag on fixed particles in turbulent flow and compare the results to drag models. Particles have dimensions  $d_p/\eta = 1.53 - 9.59$  and are subjected to meanflow with free-stream turbulence ranging from 10-25% ( $Re_p=60-600$ ). They find that drag models of the form of equation (2) work well for predicting the time-averaged forces for small particles. They also show that such drag models perform reasonably well for predicting instantaneous forces experienced by small particles, as long as the correct instantaneous slip velocity is used.

As particle size and turbulence level is increased, Bagchi & Balachandar find that the neither drag models given by equations (2) or (3) are able to capture drag fluctuations observed in the DNS. Adding history terms derived by [7] does not improve the predictions, but rather introduces unphysical oscillations in the predicted drag. An obvious hurdle they face in testing the drag model is choosing a definition of instantaneous slip velocity. This is because the large particle size and the multiscale

nature of turbulence prevent an objective definition of local and undisturbed flow velocities. In this case drag coefficients become dependent on the choices of the volume around which averages are performed. Another problem is that the kernels used to compute history terms were derived assuming small Reynolds numbers and slowly varying slip-velocities, which is not valid when turbulence intensity is high and particles are large.

These results indicate that we must reconsider both drag models and the definition of characteristic slip velocities for the case of large particles in turbulent flows. A possible approach is to model turbulent drag as a combination of steady and fluctuating terms. Earlier we defined  $U_s$  as the difference between ‘appropriate’ fluid and particle velocities. To perform a Reynolds decomposition, we work with expectation values  $\langle \cdot \rangle$ , which practically are approximated as averages over a sufficiently large statistically homogeneous region in space and/or a statistically steady period in time. We perform the Reynolds decomposition on instantaneous fluid velocities  $u_f$  and instantaneous particle center of mass velocities  $u_p$ . The residuals  $u'_f$  and  $u'_p$  can be found from the instantaneous values  $u_i - \langle u_i \rangle$ , but we note that co-located values  $u'_p - u'_f$  are only clearly defined if  $\langle \cdot \rangle$  is replaced with a spatial filtering operation. For the remainder of the work presented here,  $\langle \cdot \rangle$  is sufficient for our purposes. Thus, performing a Reynolds decomposition on the slip velocity gives  $U_s = (\langle u_f \rangle - \langle u_p \rangle) + (u'_f - u'_p) = \langle u_s \rangle + (u'_f - u'_p)$ . We can use the two slip velocities to decompose drag into steady and fluctuating terms:

$$F_D = F + G, \quad (4)$$

$$F_D = \alpha \langle u_s \rangle \beta (\langle u_s \rangle) + G, \quad (5)$$

where the effect of the fluctuating component of the slip velocity ( $u'_f - u'_p$ ) is included in  $G$ . The steady term has been shown to work relatively well in some cases [10, 11], thus  $G$  can be considered either a correction term or a noise term [12, 13]. It can be formulated in analogy to the standard drag law:

$$G = \alpha (u'_f - u'_p) \beta (u'_f - u'_p) \quad (6)$$

Or given its own formulation

$$G = f(u'_f, u'_p, d_p, \rho_f, \mu_f, \dots) \quad (7)$$

$G$  can be deterministic, but that carries the same problems as specifying  $F_D$ . Alternatively,  $G$  can be considered a stochastic term. Because the idea of slip velocity is compelling to our intuition, and related to the idea of a relaxation time, we would like to identify a single velocity scale to use in  $f$  that will describe the stochastic “slip” between particle and fluid velocity fluctuations.

### 3. Stochastic slip velocity

Two obvious choices for the stochastic slip velocity  $V$  are:

$$V_A \equiv (\langle u_f'^2 \rangle - \langle u_p'^2 \rangle)^{1/2} \quad (8)$$

and

$$V_B \equiv \langle (u'_f - u'_p)^2 \rangle^{1/2}. \quad (9)$$

We consider both of these definitions. One immediate advantage of  $V_A$  is that it can be determined by measuring the fluid and particle phase velocity statistics independently. In contrast,  $V_B$  includes a covariance  $\langle u'_f u'_p \rangle$ . An advantage of  $V_B$  is that it arises naturally from equation 6, being the variance of the instantaneous slip  $u'_f - u'_p$ . A third option,  $V_C \equiv \langle u'^2_f \rangle^{-1/2} - \langle u'^2_p \rangle^{-1/2}$ , is an algebraic variation on  $V_A$ . We prefer  $V_A$  over  $V_C$  because  $V_A$  can be easily visualized as the difference between the power spectrum of particle velocity and the power spectrum of the fluid phase velocity. In addition,  $V_A$  can be calculated equally well for laboratory, field, and numerical experiments.

To understand the behavior of  $V_A$  and  $V_B$ , we consider two extreme cases. A passive tracer, by definition, will have  $\langle u'^2_p \rangle = \langle u'^2_f \rangle = \langle u'_f u'_p \rangle$ . In this case, both stochastic fluctuating slip velocities will be zero:  $V_A = V_B = 0$ . The other extreme is a particle that does not respond to any of the fluctuating fluid velocities. This may be because the particle is anchored at a location, or because it moves “ballistically” through the flow with large inertia. By this definition, this extreme case has  $u'_p = 0$ , which makes  $\langle u'_f u'_p \rangle = 0$  as well. Thus in this extreme case both our definitions of slip velocity equal the magnitude of velocity fluctuations in the fluid phase:  $V_A = V_B = \langle u'^2_f \rangle^{1/2}$ . Both of these limiting behaviors (totally passive and totally ballistic) yield stochastic fluctuating slip velocities that make good sense: passive particles do not slip relative to the fluid phase, while 100% of the turbulent fluctuations slip past ballistic particles.

We can also use these limiting behaviors to provide a constraint that can help us prescribe models for  $\langle u'_f u'_p \rangle$ . We start with the assumption that  $\langle u'_f u'_p \rangle = f(\langle u'^2_f \rangle, \langle u'^2_p \rangle)$ . Nondimensionalizing by  $\langle u'^2_f \rangle$  gives  $\frac{\langle u'_f u'_p \rangle}{\langle u'^2_f \rangle} = F\left(\frac{\langle u'^2_p \rangle}{\langle u'^2_f \rangle}\right)$ . The limiting behaviors discussed above imply that  $F(0) = 0$  and  $F(1) = 1$ . The simplest function satisfying these constraints is linear:  $F(x) = x$ . This choice implies that the covariance equals the particle velocity variance, which makes the definitions for  $V_A$  and  $V_B$  identical. Until proper data is available to support a more complex model for the covariance, we will assume that this simple model is acceptable. This leaves us with a single definition of stochastic slip velocity:  $V = V_A \approx V_B$ . We analyze  $V$  using laboratory data below.

## 4. Experiment

Experiments are performed in a turbulent water tank, which uses two symmetric arrays of randomly firing synthetic jets to generate homogeneous isotropic turbulence with almost zero mean flow [14]. All measurements are taken within the region of isotropy and homogeneity, which is a cube roughly 30 cm on each side. In this region, the longitudinal integral length scale  $\Gamma_x = 7.5 \times 10^{-4}$  m, turbulent kinetic energy  $q^2 = 2.32 \times 10^{-4}$  m<sup>2</sup>s<sup>-2</sup>, dissipation rate is  $\epsilon = 1.52 \times 10^{-5}$  m<sup>2</sup>s<sup>-3</sup> and the Taylor-scale Reynolds number  $R_\lambda = 160$ . The facility is described in detail in [15, 16].

	$(d_p, l_p)/\eta$	$(d_p, l_p)/\lambda_x$	$(d_p, l_p)/\Lambda_x$	$\tau_p/\tau_\eta$	$\tau_p/T$
<i>Spheres</i>	21, 21	0.65, 0.65	0.11, 0.11	26	1.1
<i>Ellipsoids</i>	21, 42	0.65, 1.3	0.11, 0.22	39	1.6

**Table 1.** Relevant particle parameters relative to turbulent scales.

A suspension of large near-neutrally buoyant particles is studied at a volume fraction of 0.14%. Particles' density  $\rho_p = 1020\text{kg/m}^3$  at 20°C and they are manufactured by hand using injection molding. Particles are made of a transparent hydrogel solution, closely matched to the refractive index of water. Each particle contains hundreds of small ( $\approx 40\ \mu\text{m}$ ) optical tracers, allowing velocities to be measured within each particle by tracking the tracers.

Two particle shapes are considered here: spheres of diameter  $d_s = 8\ \text{mm}$ , and prolate ellipsoids with polar and equatorial axes  $l_e = 16$  and  $d_e = 8\ \text{mm}$ , respectively. These particle sizes are within the inertial subrange of ambient turbulence, between the Kolomgorov microscale ( $\eta = 0.38\ \text{mm}$ ) and the integral lengthscale ( $\Gamma_x = 75\ \text{mm}$ ), and of similar size to the Taylor microscale ( $\lambda_x = 16\ \text{mm}$ ). More details are given in table 1.

Although Stokes-based particle relaxation time is not useful for predicting the dynamics of particles of this size, we calculate it here as a point of reference. The Stokes-flow relaxation time of the spherical particles is  $\tau_{ps}^{(s)} = 3.64\ \text{s}$ . The Stokes-flow relaxation time of the ellipsoidal particles is computed using the expression for the average drag coefficient of randomly oriented prolate ellipsoids found in Clift *et al.* [5]:

$$C_{el} = 3\pi d_e \frac{\sqrt{a^2 - 1}}{\log(a + \sqrt{a^2 - 1})}, \quad (10)$$

where  $a = l_e/d_e$  is the particle aspect ratio. Consequently, the particle response time for our ellipsoids of  $a = 2$  and  $d_e = d_s$  becomes:

$$\tau_{ps}^{(e)} = \tau_{ps}^{(s)} a \frac{\log(a + \sqrt{a^2 - 1})}{\sqrt{a^2 - 1}} = 1.5\tau_{ps}^{(s)} \quad (11)$$

where  $\tau_{ps}^{(s)}$  is based on the smaller (equatorial) diameter of the ellipsoid. Our ellipsoidal particles thus have  $\tau_{ps}^{(e)} = 5.46\text{s}$ . According to [5], we can define an equivalent diameter  $d_p^{(eq)}$  for ellipsoidal particles as the diameter of a sphere having the same average drag coefficient as the ellipsoid. This can be determined from equation 10 to be  $d_p^{(eq)} = 10.5\ \text{mm}$ . Equation (11) offers an interesting insight on the effect of particle shape: particle response time is the ratio between inertial and drag force; while this ratio scales with particle size for spheres, this is not true for elongated particle. For example, increasing particle size by increasing the aspect ratio might actually decrease the response time and the equivalent diameter.

Fluid phase velocity measurements are performed using standard 2D particle image velocimetry (PIV). These measurements use a single camera oriented perpendicular to a measurement volume of dimensions 4 cm x 3.4 cm x 0.1 cm centered in the tank.

	Input velocity:	$u_p^{(s)}$	$u_p^{(e)}$	$u_f$	$\overline{(u_f)_d}$	$\overline{(u_f)_l}$
$\langle u^2 \rangle$	$\times 10^{-4} \text{ [m}^2/\text{s}^2]$	1.38	1.09	1.55	1.46	1.38
$\langle u^4 \rangle / \langle u^2 \rangle^2$	[-]	4.28	4.94	3.06	2.66	2.57

**Table 2.** Second and fourth order statistics of particle and fluid phase velocity.

The final size of the interrogation area is  $32 \times 32$  pixels, corresponding to  $0.8 \times 0.8$  mm in physical space. This size is on the order of  $2\eta$ , thus spatial resolution effects are expected to be negligible. Statistics of the fluid phase are based on 510 independent velocity fields (corresponding to  $> 300$  integral time scales) containing  $102 \times 86$  datapoints each.

We measure velocities within particles using stereoscopic PIV. The optical setup is two cameras (Imager PRO-X,  $1600 \times 1200$  pixels, both fitted with a 50 mm Nikkor lens and Scheimpflug/tilt adapter) viewing a 1mm thick laser light sheet, capturing a measurement volume of 14 cm x 8 cm x 0.1 cm centered in the tank. The two cameras view the measurement area from opposite sides, each at an angle of 35 degrees relative to the laser’s forward-scatter direction. From the velocities within each particle, we compute linear and angular velocities of the particles (see Appendix). Statistics of angular velocity are not presented here, but they are important when measuring large particles. For example, we have used them to control error in the linear velocity measurements (see Appendix). Statistics of particle velocity are obtained from 927 and 1076 trajectories for spheres and ellipsoids, respectively. More details on the experimental setup and measurement techniques are given in [17].

## 5. Result

The probability density functions (*pdfs*) of particles’ linear velocities ( $u_p$ ) are shown in figure 1a. For both spheres and ellipsoids, the *pdfs* are symmetric around  $u_p = 0$ , as expected for homogeneous isotropic turbulence with zero mean flow. Table 2 shows that both particle types have velocity variance that is significantly smaller than that of the fluid phase. This is an immediate indication that particles do not behave as passive tracers. The variance of ellipsoidal particle velocities is significantly lower than that for spheres, implying that they follow the flow less faithfully than the spheres, likely due to their shape or to their longer relaxation timescale (ellipsoids’ Stokes-based response time is 50% longer than spheres, as derived in section 4).

Figures 1b and 1c compare the particle velocity *pdfs* to the fluid phase velocity. We include *pdfs* of the velocity field filtered at lengthscales corresponding to the spherical particle diameter ( $\overline{(u_f)_d}$ ) and the ellipsoids’ major axis ( $\overline{(u_f)_l}$ ). Comparison with these demonstrates the nonlinear dynamics of particle-turbulent interactions, as discussed below. When particles show preferential concentration, they selectively sample the fluid velocity field [18, 19, 20]. Based on the results of [21], we do not expect that our particles will behave in such a way, and thus we assume that they uniformly sample the velocity field. If not, the particle *pdfs* should be compared to fluid velocity statistics conditioned

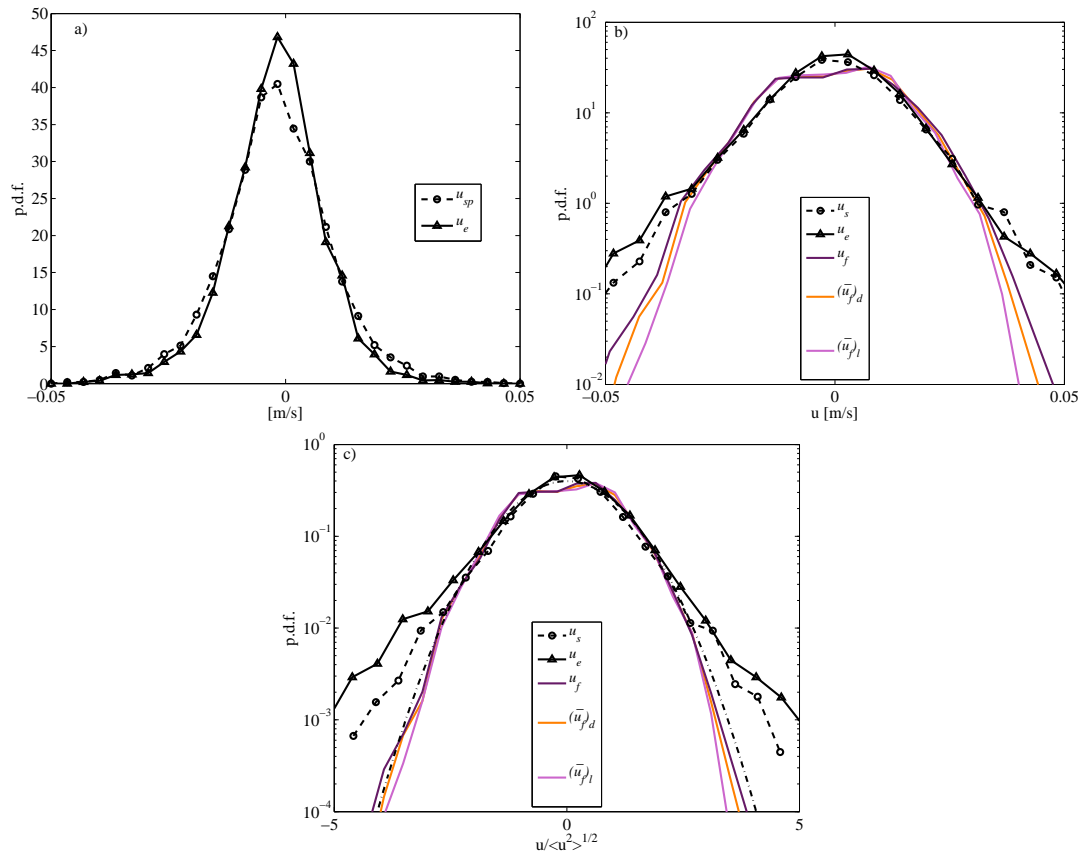


**Figure 1.** a) Histograms of spherical (solid lines) and ellipsoidal (dashed lines) particles' velocity components. b) Comparison with fluid velocity *pdfs*. c) Normalized pdf showing hyper-gaussianity of particle velocity. The figure shows that particle velocity is not trivially related to velocity at any scale.

on vorticity [22].

The shape of the normalized *pdfs* seen in figure 1c is of particular interest, because it reveals whether particles simply act as a linear filter of the velocity field, or if the interaction is more complex. From figure 1c we can see that while fluid velocity follows a nearly gaussian distribution, particles show a super-gaussian behavior, which is even more pronounced for ellipsoidal particles. We quantify this effect with fourth order moments of the *pdfs*, see table 2). This indicates that the filtering relationship between particle and fluid velocity is nonlinear, as is discussed further in section 6.

Applying the definition of slip velocity given in equation (9) we obtain that slip velocity for spherical particles is  $V^{(s)} = 4$  mm/s and for ellipsoidal particles is  $V^{(e)} = 6.8$  mm/s. The definition of stochastic slip velocity  $V$  can also be modified to so that it uses the variance of a spatially filtered fluid velocity field. The advantage of doing this is that it could explicitly represent the manner in which particles spatially filter the fluid velocity field. Doing so also provides an unambiguous definition for the covariance term in  $V_B$ . However, it is not yet known what filter best approximates the particles experience of the fluid velocity field. Indeed, if this were known, it would be an important



	Slip velocity $V$	$(\langle u_f^2 \rangle - \langle u_p^2 \rangle)^{1/2}$	$(\langle \overline{(u_f)_d}^2 \rangle - \langle u_p^2 \rangle)^{1/2}$	$(\langle \overline{(u_f)_l}^2 \rangle - \langle u_p^2 \rangle)^{1/2}$
<i>Spheres</i>	$\times 10^{-3}$ [m/s]	4.0 ( $Re_p=32$ )	2.8 ( $Re_p=22$ )	0 ( $Re_p=0$ )
<i>Ellipsoids</i>	$\times 10^{-3}$ [m/s]	6.8 ( $Re_p=69$ )	6.2 ( $Re_p=63$ )	5.4 ( $Re_p=55$ )

**Table 3.** Slip velocities and particle Reynolds numbers.

step forward in modeling fluctuating drag on large particles in turbulence. Here, we use a simple boxcar filter, and find that the slip velocity does not change significantly with this filtering (see table 3). This is likely because the variance is a large-scale statistic and particles are at the Taylor microscale. Filtering the fluid at progressively larger scales will eventually cause the slip velocity to become negative. Apparently by coincidence, we have found that this critical filter size for spherical particles in our flow is twice the sphere diameter.

We can use the stochastic slip velocity  $V$  to define a Reynolds number  $Re_V \equiv V d_p \nu^{-1}$ . For the particles measured here,  $Re_V$  is 32 for spheres and 69 for ellipsoids. We consider this result the first indication that  $Re_V$  may indicate the degree of nonlinearity in the particle fluid interactions. This hypothesis is driven by two observations. First, as  $Re_V$  approaches zero, the fluid particles follow the flow as passive tracers, and thus their motion is a linear function of the fluid phase velocity. Second, the particles measured here have  $Re_V > 1$ , demonstrate a nonlinear response to the fluid velocity field (as indicated by the *pdfs*), and the strength of this nonlinearity is correlated with the Reynolds number (*i.e.* ellipsoids have a larger  $Re_V$  and exhibit greater nonlinearity). Of course, this correlation is based on only two points in parameter space, and our assumptions about how  $Re_V$  should indicate drag linearity are based primarily on analogy with the particle Reynolds number in Stokes flow. Thus more analysis is needed to understand the meaning of  $Re_V$ , which we expect will be closely tied to the development of stochastic drag models employing  $V$ .

## 6. Discussion

The kurtosis and scaled *pdfs* of particle velocities show that large particles like the ones used here exhibit super-gaussian behavior. The significance of super-gaussian behavior is that it indicates intermittency. Intermittent behavior is typically seen in small-scale turbulent processes [23, 24, 25] and thus the intermittency in particle dynamics may help identify links between particle motion and fluid flow. Super-gaussianity of large spherical particles was also reported by Qureshi *et al.* [4]. In their experiments, intermittent behavior persists for particle sizes up to the largest turbulent scales, while fluid velocity increments at the scale of large particles are nearly gaussian. This indicates a non-trivial link between particle and fluid velocity. They suggest that particle acceleration statistics are related to statistics of the eulerian pressure increment, which indeed is a complex function of the velocity field.

Particle velocity intermittency also appears to depend on particle shape. Our

data show that intermittent behavior is more pronounced for ellipsoidal particles than for spheres. We attribute this difference at least partially to shape, because the ellipsoids considered here have an equivalent diameter similar to the spheres' diameter ( $d_p^{(e)} = 1.3d_p^{(s)}$ ). Unlike spheres, ellipsoids have orientation-dependent drag. That is, in equation 1, the drag must also include orientation  $\phi$ :  $F_D^{(e)} = f(Re_p, \phi(t), \dots)$ . As orientation fluctuates, so will the drag coefficient.

The difference between the scaled particle and fluid *pdfs* in figure 1c might help point the way to an improved use of Stokes number for large particles in turbulent flow. The Stokes number is successful in predicting particle dynamics and turbulence modulation for small particles in turbulent flow [3, 8, 26]. When particles become large, then the Stokes number fails in two ways. First, the assumptions inherent in its derivation become invalid. Second, it fails to collapse dynamics across a wide range of flows. Lucci *et al.* [27] examined this failure, showing that large particles with identical values of Stokes number had very different behaviors. Similar problems with Stokes number are also seen for dense particles, but due to different physical effects, and are discussed in [28].

The definition of Stokes number uses an exponential particle relaxation timescale, which follows from a drag law that is linear in  $U_s$ . If the steady drag  $F$  is similarly linear in  $\langle u_s \rangle$ , then an analogous result will follow. This is essentially what Xu & Bodenschatz [21] propose. They formulate a Stokes number that is the ratio of to a filtered turbulent timescale and particles' response time to a filtered velocity field.

The fact that particle velocities do not follow the filtered velocity field (as seen in fig. 1) implies that either  $F$  is nonlinear,  $G$  is non-negligible, or both. As a result we can predict that the filtered Stokes number will not effectively collapse dynamics that depend on the sub-filter scale motions. Notable effects that will depend on these motions are particle clustering and turbulence modulation.

At this stage, we see three main uses for our definition of stochastic slip velocity  $V \equiv (\langle u_f^2 \rangle - \langle u_p^2 \rangle)^{1/2}$ . The first is to quantify the importance of fluctuating drag  $G$ . When  $V = 0$ , the particle acts as a tracer and thus  $G = 0$ . When  $V$  is nonzero, we can compare it to the steady slip velocity  $\langle u_s \rangle$ , to understand the relative importance of steady and fluctuating slip. As these slips enter into the steady and fluctuating drag ( $F$  and  $G$ ) respectively, we can infer that  $F/G$  is a function of  $\langle u_s \rangle/V$ . Rather than comparing the slip velocities directly, we can also compare their equivalent Reynolds numbers:  $Re_V \equiv (\langle u_f^2 \rangle - \langle u_p^2 \rangle)^{1/2} d_p \nu^{-1}$  and  $Re_s \equiv (\langle u_f \rangle - \langle u_p \rangle) d_p \nu^{-1}$ .

The second major use for  $V$  is as an input for formulating  $G$ . There are many possible expressions for  $G$ , but we expect they all will include a comparison of  $\langle u_f^2 \rangle$  and  $\langle u_p^2 \rangle$ . We suggest that the difference  $V$  is preferable to the ratio  $\langle u_f^2 \rangle \langle u_p^2 \rangle^{-1}$  because its form is analogous to the slip velocity that shows up in the standard and steady drag laws. Future work, primarily DNS, will be needed before the exact relationship between  $G$  and  $V$  can be determined.

The third major use for  $V$  is in predicting some of the key features of particle-laden turbulent suspensions. There is currently no method for predicting turbulence

modulation (such as TKE amplification or attenuation) and particle clustering (*i.e.* preferential concentration) for suspensions of large particles in turbulence. For small particles, the Stokes number has been used to predict these effects, but it fails for large particles as discussed above. We expect that whatever non-dimensional parameters predict clustering and TKE modulation for large particles will also control the stochastic slip velocity  $V$ . If this is true, then  $V$  could serve as a midway predictor for clustering and TKE modulation. This would serve two purposes:  $V$  may be easier to measure than the clustering and TKE modulation, and the relationship between  $G$  and  $V$ , once found, would guide the search for a predictor of clustering and TKE modulation.

## 7. Conclusions

The standard drag model fails to accurately describe forces on large particles in turbulent flows. We can replace the standard drag with the sum of steady and fluctuating drag terms, but the fluctuating drag term has not yet been parameterized. Herein, we discuss the definition of a stochastic slip velocity. This can serve as an input to fluctuating drag models, and also serve other key analyses in turbulent particle suspension dynamics. Specifically, it allows us to determine a particle Reynolds number for neutrally buoyant particles, and contributes to the extension of the Stokes number. This is essential for efforts to accurately predict the dynamics of large particles in turbulent flows.

We discuss two options for the stochastic slip velocity, and demonstrate their approximate equivalence. We then measure the stochastic slip velocity using laboratory data collected on large ellipsoidal and spherical particles in homogeneous isotropic turbulence. The results suggest that particle Reynolds number based on the stochastic slip is an effective predictor of nonlinear fluid–particle interactions. Specifically, both particles show velocity distributions with greater kurtosis than the fluid phase velocity distribution. Comparing the ellipsoids and spheres, we see that the increase in kurtosis is correlated with an increase in particle Reynolds number.

A key next step is to extend this argument to filtered, rather than expectation, velocities. This will allow us to quantify the covariance between velocity and fluid fluctuations, and thus evaluate the difference between our two proposed definitions of stochastic slip velocity ( $V_A$  and  $V_B$ ). In addition, we can evaluate rotational slip by using within-particle velocities to extract particle rotation measurements.

## Appendix

We use stereoscopic PIV to measure the velocities  $\mathbf{U}_M$  and  $\mathbf{U}_N$  at two points within the particle:  $\mathbf{X}_M$  and  $\mathbf{X}_N$ . From these measurements the angular velocity  $\boldsymbol{\Omega}$  can be determined from the equation of solid body rotation:

$$\mathbf{U}_N = \mathbf{U}_M + \boldsymbol{\Omega} \times (\mathbf{X}_N - \mathbf{X}_M). \quad (12)$$

Since PIV measurements are in a single  $x - y$  plane, equation 12 is over-determined in  $\Omega_z$  and under-determined in  $\Omega_x$  and  $\Omega_y$ . By including a third point  $P$  in addition to  $M$

and  $N$ , all three components of  $\boldsymbol{\Omega}$  can be determined.

Because PIV provides many more than 3 velocities within each particle, we can improve the precision and accuracy of  $\boldsymbol{\Omega}$  measurements. We do this by calculating a value of  $\boldsymbol{\Omega}$  using each possible set of three points  $M$ ,  $N$  and  $P$ , and considering the distribution of  $\boldsymbol{\Omega}$  estimates.

The location of the particle center of gravity is not explicitly measured by PIV, but the velocity there ( $\mathbf{V}_{\text{cg}}$ ) can be determined as follows. The equation of solid body rotation gives:

$$\mathbf{V}_{\text{cg}} = \mathbf{V}_{\text{cf}} - \boldsymbol{\Omega} \times \mathbf{r}, \quad (13)$$

where  $\mathbf{V}_{\text{cf}}$  is the velocity at the center of the particle cross-section formed by the intersection of the particle and the PIV measurement plane,  $\boldsymbol{\Omega}$  is the angular velocity as calculated above, and  $\mathbf{r} = (r_x, r_y, r_z)$  is the distance between the center of gravity of the particle and the center of the particle cross-section. Note that for spherical particles  $r_x = r_y = 0$ . From equation (13), we can express the variance of  $\mathbf{V}_{\text{cg}}$  as:

$$\langle \mathbf{V}_{\text{cg}}^2 \rangle = \langle \mathbf{V}_{\text{cf}}^2 \rangle - \langle (\boldsymbol{\Omega} \times \mathbf{r})^2 \rangle - \langle 2\mathbf{V}_{\text{cf}}(\boldsymbol{\Omega} \times \mathbf{r}) \rangle. \quad (14)$$

It is reasonable to assume that the last term on the RHS of equation 14 vanishes because the velocity of the center of gravity and the velocity induced by particle rotation at the measurement location are uncorrelated. We therefore are left with the expression:

$$\langle \mathbf{V}_{\text{cg}}^2 \rangle = \langle \mathbf{V}_{\text{cf}}^2 \rangle - \langle (\boldsymbol{\Omega} \times \mathbf{r})^2 \rangle. \quad (15)$$

This indicates that the variance of the velocity at the particle's center of gravity is the variance of the velocity measured at the center of a randomly oriented plane intersecting the particle minus the 'rotation-induced noise term  $\langle (\boldsymbol{\Omega} \times \mathbf{r})^2 \rangle$ ' that is due to the velocity induced by particle rotation at the measurement point.

To quantify the importance of the rotation-induced noise term, we expand  $\mathbf{V}_{\text{rin}} = \boldsymbol{\Omega} \times \mathbf{r}$  in its components. Because spherical particles have  $r_x = r_y = 0$ , the noise term becomes  $(u_{\text{rin}}, v_{\text{rin}}, w_{\text{rin}}) = (\Omega_y r_z, -\Omega_x r_z, 0)$ . Therefore, we can immediately conclude that the variance of  $w_{\text{cf}}$  equals the variance of  $w_{\text{cg}}$ . The variance of the other two components can be expanded by noting that the vector  $\boldsymbol{\Omega}$  is independent of  $r_z$ . Therefore we can express the variance of the products as the product of the variances:  $\langle (\Omega_i r_z)^2 \rangle = \langle \Omega_i^2 \rangle \langle r_z^2 \rangle$ . The variance of the distance  $r_z$  of a point chosen randomly within the volume of a spherical particle of radius  $R$  is  $\langle r_z^2 \rangle = \frac{3}{5} R^2$ . Therefore  $\langle u_{\text{rin}}^2 \rangle = \frac{3}{5} R^2 \langle \Omega_x^2 \rangle$ , and  $\langle v_{\text{rin}}^2 \rangle = \frac{3}{5} R^2 \langle \Omega_y^2 \rangle$ .

In our measurements, the diameter of spherical particles is  $R = 4 \times 10^{-3}$  m, and the angular velocity measurements show that  $\langle \Omega_i^2 \rangle = O(10^{-1})$ . Therefore the noise term is  $O(10^{-7})$ . Comparing this to  $\langle u_{\text{cf}}^2 \rangle$ , which is  $O(10^{-4})$ , we conclude that the rotation-induced noise is negligible in our measurements of spherical particles velocity variance. For ellipsoidal particles, the expression for  $\mathbf{V}_{\text{rin}}$  becomes much more complicated because  $r_x$  and  $r_y$  are non-zero and the expression for the radius variance is different than that for spheres. However, our measurements of  $\boldsymbol{\Omega}$  for ellipsoids are very similar to the results for spheres. Given this, and the fact that the ellipsoids are very similar size to

the spheres, we expect the order of magnitude of the noise term to be similar for spheres and ellipsoids. As a result, we neglect the rotation-induced noise when calculating the variance of ellipsoid velocities. Should these terms be non-negligible in other cases, they can be quantified using the method presented here.

## References

- [1] C Poelma and G Ooms. Particle-turbulence interaction in a homogeneous, isotropic turbulent suspension. *Applied Mechanics Reviews*, 59:78–89, 2006.
- [2] F Toschi and E Bodenschatz. Lagrangian properties of particles in turbulence. *Annu. Rev. of Fluid Mech.*, 41:375–404, Jan 2009.
- [3] S Balachandar and J K Eaton. Turbulent dispersed multiphase flow. *Annu. Rev. of Fluid Mech.*, 42:111–133, 2010.
- [4] N Qureshi, M Bourgoïn, C Baudet, and A Cartellier. Turbulent transport of material particles: An experimental study of finite size effects. *Physical Review Letters*, 2007.
- [5] R Clift, J R Grace, and M E Weber. Bubbles, drops, and particles. *ACADEMIC PRESS New York San Francisco London*, 1978.
- [6] M R Maxey and J J Riley. Equation of motion for a small rigid sphere in a nonuniform flow. *Phys. Fluids*, 26:883–890, 1983.
- [7] R Mei and R J Adrian. Flow past a sphere with an oscillation in the free-stream velocity and unsteady drag at finite reynolds number. *J. Fluid Mech.*, 237:323–341, 1992.
- [8] John K Eaton. Two-way coupled turbulence simulations of gas-particle flows using point-particle tracking. *Int. J. of Multiphase Flow*, 2009.
- [9] R Mei. Velocity fidelity of flow tracer particles. *Exp. in Fluids*, 22:1–13, 1996.
- [10] P Bagchi and S Balachandar. Effect of turbulence on the drag and lift of a particle. *Phys. Fluids*, 15(11):3496–3513, 2003.
- [11] E Loth. Drag of non-spherical solid particles of regular and irregular shape. *Powder Technology*, 182:342–353, 2008.
- [12] Allen Clamen and W. H. Gauvin. Effects of turbulence on the drag coefficients of spheres in a supercritical flow regime. *AIChE Journal*, 15(2):184–189, 1969.
- [13] N Moradian, D S K Ting, and S Cheng. The effects of freestream turbulence on the drag coefficient of a sphere. *Experimental Thermal and Fluid Science*, 33(3):460 – 471, 2009.
- [14] E A Variano and E A Cowen. A random-jet-stirred turbulence tank. *J. Fluid Mech.*, 604:1–32, 2008.
- [15] G Bellani, M L Byron, A G Collignon, C R Meyer, and Evan A Variano. Shape effects on turbulent modulation by large nearly neutrally buoyant particles. *Submitted*, pages 1–19, 2012.
- [16] G Bellani and E A Variano. Homogeneity and isotropy in a laboratory turbulent flow. *Unpublished working paper*, pages 1–18, 2012.
- [17] G Bellani. Experimental studies of complex flows through image-based techniques. *PhD Thesis, Royal Institute of Technology, Stockholm*, 2011.
- [18] J K Eaton. Preferential concentration of particles by turbulence. *Phys. Fluids*, 3(5):1169–1178, 1991.
- [19] M Gibert, H Xu, and E Bodenschatz. Where do small, weakly inertial particles go in a turbulent flow? *J. Fluid Mech.*, First View:1–8, 2012.
- [20] I Fouxon. Distribution of particles and bubbles in turbulence at a small stokes number. *Physical Review Letters*, 108(13):1–5, 2012.
- [21] H Xu and E Bodenschatz. Motion of inertial particles with size larger than kolmogorov scale in turbulent flows. *Physica D*, 237:2095–2100, 2008.
- [22] P H Mortensen, H I Andersson, J J J Gillissen, and B J Boersma. Dynamics of prolate ellipsoidal particles in a turbulent channel flow. *Phys. Fluids*, 20:0933202, 2008.

- [23] A Tsinober. An informal introduction to turbulence. *Kluwer academic publisher*, 2004.
- [24] L Biferale, G Boffetta, A Celani, B Devenish, A Lanotte, and F Toschi. Multifractal statistics of lagrangian velocity and acceleration in turbulence. *Physical Review Letters*, 93(6):1–4, 2004.
- [25] J Bec, L Biferale, M Cencini, A Lanotte, and F Toschi. Effects of vortex filaments on the velocity of tracers and heavy particles in turbulence. *Phys. Fluids*, 18:081702, 2006.
- [26] S Elghobashi. On predicting particle-laden turbulent flows. *Applied Scientific Research*, 52:309–329, 1994.
- [27] F Lucci, A Ferrante, and S Elghobashi. Is stokes number an appropriate indicator for turbulence modulation by particles of taylor-length-scale size? *Phys. Fluids*, 23(2):025101, 2011.
- [28] T Tanaka and J K Eaton. Classification of turbulence modification by dispersed spheres using a novel dimensionless number. *Physical Review Letters*, 101(11):1–4, 2008.